Fluid Antenna System—Part III: A New Paradigm of Distributed Artificial Scattering Surfaces for Massive Connectivity

Kai-Kit Wong, *Fellow, IEEE,* Kin-Fai Tong, *Fellow, IEEE,* and Chan-Byoung Chae, *Fellow, IEEE*

***Abstract*—Reconfigurable intelligent surface (RIS) has recently emerged as a promising technology to extend the coverage of a base station (BS) in wireless communication networks. However, the adoption of RIS comes with the challenges of highly complex joint optimization of the multiple-input multiple-output (MIMO) precoding matrix at the BS and the phase shifters of the RIS as well as estimation of the cascaded channels. To circumvent this, this letter presents a new paradigm that uses RISs as distributed artificial scattering surfaces (DASSs) to produce a rich scattering environment that enables fluid antenna system (FAS) to prevent multiuser interference at each user equipment (UE). The use of fluid antenna multiple access (FAMA) liberates MIMO and RIS and greatly simplifies their optimization. Our simulation results show that with DASS, slow FAMA can obtain a high multiplexing gain without precoding and phase shifter design when the direct link does not exist. In the presence of the direct link, nonetheless, BS precoding becomes essential. Our results further reveal that fast FAMA with 20 DASSs can accommodate 64 co-channel UEs to achieve a multiplexing gain of 59.3 without precoding at the BS nor RIS phase shifter optimization and the direct link.**

***Index Terms*—Artificial scattering, fluid antenna system, massive connectivity, reconfigurable intelligent surface.**

I. Introduction

A. Motivation

THE fifth-generation (5G) New Radio (NR) has turned to higher frequency bands for larger quantities of spectrum and capacity and supports up to 60 GHz (i.e., V-band). There has also been strong interest about using the terahertz bands (≥ 100 GHz) in the being developed sixth-generation (6G) [1]. Higher frequency unfortunately means shorter distance. It was reported that in terms of power consumption, 5G is between two and four times greater than 4G. Huawei estimated that the total power consumption by telecom networks will reach 100 billion kWh, a figure doubling the pre-5G era [2].

5G technologies are evidently much more energy efficient than 4G under the same traffic conditions. However, to restore coverage in the higher frequency bands, network densification becomes necessary to bring base stations (BSs) or remote radio heads (RRHs) closer to user equipments (UEs) [3], causing a huge increase in the energy footprint and power consumption. To counter this problem, in recent years, reconfigurable intelligent surface (RIS) has emerged as a possible solution.

RIS offers a large aperture to capture radio waves and intelligently redirects them to/from the intended UEs by adapting the reflection coefficients of the radiating elements (a.k.a. unit cells) [4], [5]. A key advantage of RIS is that it does not need power-hungry amplifiers that require dedicated power supply. With advances in low-power electronics, perpetual operation of RIS has even been suggested [6]. Thus, network densification may be partly achieved via RIS deployment.

However, the recent trend of RIS research seems to take a different approach and demand a lot of power consumption in signal processing and computation. To obtain the performance gain, there is a need to jointly optimize the precoding matrix at the BS and the phase shifters at the RIS [4], [5], let alone the acquisition of channel state information (CSI) of the cascaded channel. Note that the 5G Type II NR multiuser multiple-input multiple-output (MIMO) precoder is already complicated [7] and incorporating the RIS phase shifters optimization will be extremely difficult. Furthermore, the beamforming-based RIS approach is hardly scalable because if there are more than one RISs in the vicinity, the phase shifters of all the RISs need to be coordinated.[1] On the other hand, [8] warned that RIS can be adversarial and easily present a security risk.

B. New Paradigm

Following the first two parts of this letter, we present a new paradigm that reinvents RIS to collaborate with fluid antenna system (FAS). In this paradigm, RISs serve as distributed artificial scattering surfaces (DASSs) that provide the conditions desirable for fluid antenna multiple access (FAMA). As such, joint optimization of the phase shifters of the RISs is no longer required and RISs safely coexist without coordination. Fig. 1 illustrates such scenario where a MIMO BS communicates to several FAS-aided UEs in the presence of many DASSs.[2] As a matter of fact, the importance of BS precoding is also much reduced in this setup (unless the direct link is present) because the 'natural' interference null is exploited at the UEs.

FAS represents novel flexible radiating structures to enable position-switcheable antennas [9]. FAMA is a multiple access scheme in which the UEs employ FAS to find and access the spatial opportunity of the interference null produced naturally by the propagation environment [10], [11]. A brief review of FAS has been provided in the first part of this letter [12]. In [12], we also demonstrated that in the two-user case, FAMA outperforms the Han-Kobayashi (HK) scheme, suggesting that FAMA have potential for extreme massive connectivity.

In this finale of the three-part letter, our aim is to investigate the performance of FAMA when it is applied in the MIMO downlink in the presence of RISs. We are interested in finding out if RISs as DASS contribute to improving the performance of FAMA and whether precoding at the BS is really necessary

The work of Wong and Tong is supported by the Engineering and Physical Sciences Research Council (EPSRC) under Grant EP/W026813/1. For the purpose of open access, the authors will apply a Creative Commons Attribution (CC BY) licence to any Author Accepted Manuscript version arising.

The work of C. B. Chae is supported by the Institute of Information and Communication Technology Promotion (IITP) grant funded by the Ministry of Science and ICT (MSIT), Korea (No. 2021-0-02208, No. 2021-0-00486).

K. K. Wong, and K. F. Tong are with the Department of Electronic and Electrical Engineering, University College London, Torrington Place, WC1E 7JE, United Kingdom. *Corresponding author:* kai-kit.wong@ucl.ac.uk.

K. K. Wong and C. B. Chae are with Yonsei Frontier Laboratory and School of Integrated Technology, Yonsei University, Seoul, 03722, Korea.

[1] An unmanaged RIS will mess up the signal quality of the nearby UEs. In addition, an RIS cannot be stopped for 'unwanted' passive reflection.

[2] In this letter, the terms 'RIS' and 'DASS' are used interchangeably because RIS is functioning as DASS without optimization of the phase shifters.

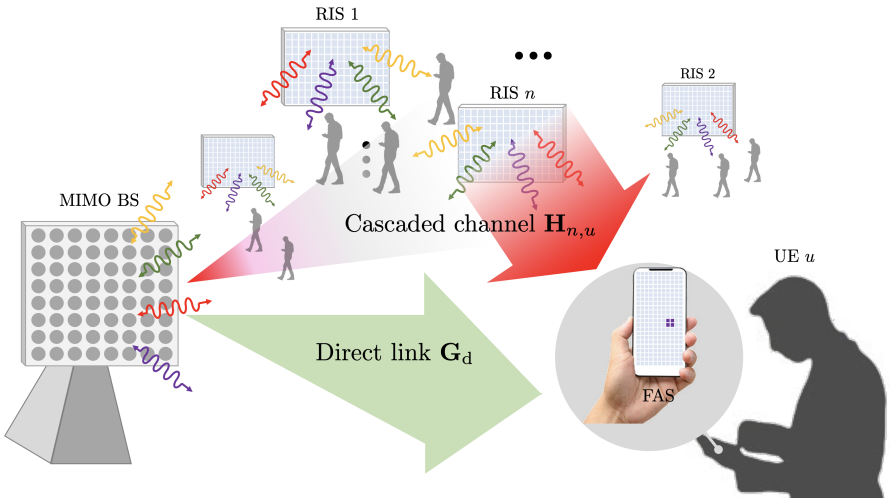

Fig. 1. A downlink system with a MIMO BS communicating to many FAS-aided UEs supported by many RISs serving as DASS.

for desirable performance. The focus will be on the millimeter wave (mmWave) bands where RIS deployment is expected to recover the range. To model the channel, we adopt the spatial scattering model in [5] which is originated from [13]. Besides, we utilize the sectoring concept in [14] to model the random angle-of-departure (AoD) and angle-of-arrival (AoA) of each channel path to and from an RIS in the mmWave band.

C. Highlight of Results

Assuming a one-dimensional (1D) $W\lambda$-long FAS with one activated port at each UE where λ denotes the wavelength, our results disclose the following properties for the MIMO-FAMA downlink when RISs act as DASS.

- The normalized size W of FAS is essential in the performance of FAMA. Higher frequency thus usually delivers better performance as the FAS affords a larger space.
- However, higher frequency tends to have a more directional channel (narrower AoDs) from the BS to the RISs, which increases correlation among different UE channels and hence hinders slow FAMA to avoid interference.
- The number of unit cells, N_{cell}, on a DASS does not need to be large and a few unit cells perform as well as many in terms of generating differences in the UE channels for slow/fast FAMA. It is much more effective to have more DASSs, N_{ris}, than more unit cells on a DASS.
- Precoding at the BS is only indispensable for slow FAMA and only when the direct link between the BS and UEs is present. In this case, choosing the principal right singular vector of the direct-link channel matrix as the precoding vector for the UE outperforms that of the overall cascaded channel matrix. In other words, even when BS precoding is performed, the cascaded channel CSI is not needed.
- When the direct link exists, the presence of DASSs does little to the performance if BS precoding is employed but improves the performance greatly without precoding.
- Without the direct link, the results show that at 26 GHz, slow FAMA obtains a multiplexing gain[3] of 4.8 serving 5 co-channel UEs, with the aid of $N_{\mathrm{ris}} = 12$ DASSs. Also, at $f = 40$ GHz, the multiplexing gain is increased to 5.7 serving 6 co-channel UEs with the same N_{ris}.
- In the case of fast FAMA, the UEs can support a much higher signal-to-interference plus noise ratio (SINR) target, γ, than in slow FAMA. BS precoding is less important with and without the direct link. Most importantly, at $f = 40$ GHz, the results illustrate that a multiplexing gain of 59.3 serving 64 co-channel UEs is achieved with $N_{\mathrm{ris}} = 20$ DASSs. This figure rises to 85.4 when serving 100 co-channel UEs under the same conditions.

II. Downlink MIMO-FAMA with DASS

A. System Model

We consider a downlink system where a MIMO BS communicates to U FAS-aided UEs in the presence of N_{ris} DASSs. The BS is equipped with a uniform square array (USA) of N_t elements while each UE has a 1D $W\lambda$-long N-port FAS. The DASSs are located far apart from each other to have different AoDs from the BS and AoAs to the UEs. Every DASS has N_{cell} unit cells over a two-dimensional (2D) square grid.

With the usual assumption of an omnidirectional radiation pattern of each port at FAS and negligible port switching delay, we can write the cascaded channel matrix, $\mathbf{H}_{n,u} \in \mathbb{C}^{N\times N_t}$, between the BS and UE u via the n-th DASS using the spatial scattering model (each unit cell as a scatterer) in [5, (4)] as

$$\mathbf{H}_{n,u} = \frac{1}{\sqrt{d_1^{\alpha_1}}\sqrt{d_2^{\alpha_2}}} \sum_{m=1}^{N_{\mathrm{cell}}} e^{j\varphi_{n,m}} \times \mathbf{a}_r(\theta_{\mathrm{AoA},m}^{(n,u)}, \phi_{\mathrm{AoA},m}^{(n,u)}) \mathbf{a}_t^{\dagger}(\theta_{\mathrm{AoD},m}^{(n)}, \phi_{\mathrm{AoD},m}^{(n)}), \quad (1)$$

where d_1 and d_2 denote, respectively, the distance between the BS and DASS n and that between DASS n to the UE,[4] α_1 and α_2 are the corresponding path loss exponent, $\varphi_{n,m}$ is the resulting phase shift acted on the m-th unit cell of DASS n, $\theta_{\mathrm{AoA},m}^{(n,u)}, \phi_{\mathrm{AoA},m}^{(n,u)}, \theta_{\mathrm{AoD},m}^{(n)}, \phi_{\mathrm{AoD},m}^{(n)}$ denote, respectively, the azimuth AoA and the elevation AoA from DASS n to UE u

[3]Same as in [10], [11], we consider the case that the BS is transmitting a fixed rate to every UE and as a result, the multiplexing gain is defined as the capacity scaling based on the average outage rate.

[4]For notational simplicity and ease of our discussion, we assume the same distances from the BS to all DASSs and from every DASS to any UE.

due to the m-th unit cell, the azimuth AoD and the elevation AoD from the BS to the m-th unit cell of DASS n, and the steering vectors, $\mathbf{a}_r(\theta,\phi)$ and $\mathbf{a}_t(\theta,\phi)$, are given by

$$\mathbf{a}_r(\theta,\phi)=\left[1\ e^{j\left(\frac{2\pi W}{N-1}\right)\sin\theta\cos\phi}\cdots\ e^{j2\pi W\sin\theta\cos\phi}\right]^T \quad (2)$$

and

$$\mathbf{a}_t(\theta,\phi)=\left[1\ e^{j\pi\sin\theta\cos\phi}\cdots\ e^{j\pi(\sqrt{N_t}-1)\sin\theta\cos\phi}\right]^T \otimes\left[1\ e^{j\pi\sin\theta\cos\phi}\cdots\ e^{j\pi(\sqrt{N_t}-1)\sin\theta\cos\phi}\right]^T, \quad (3)$$

where $\otimes$ denotes the Kronecker tensor product.

For the direct-link channel, $\mathbf{G}_d^{(u)}\in\mathbb{C}^{N\times N_t}$, we can use the finite scattering model in [13] so that

$$\mathbf{G}_d^{(u)}=\frac{1}{\sqrt{d_0^{\alpha_1}}}\left[\sqrt{\frac{K}{K+1}}e^{j\delta_u}\times \mathbf{a}_r(\bar{\theta}^{(u)}_{\mathrm{AoA},0},\bar{\phi}^{(u)}_{\mathrm{AoA},0})\mathbf{a}_t^\dagger(\bar{\theta}^{(u)}_{\mathrm{AoD},0},\bar{\phi}^{(u)}_{\mathrm{AoD},0}) + \frac{1}{\sqrt{N_p}}\sqrt{\frac{1}{K+1}}\sum_{\ell=1}^{N_p}\beta_\ell^{(u)}\times \mathbf{a}_r(\bar{\theta}^{(u)}_{\mathrm{AoA},\ell},\bar{\phi}^{(u)}_{\mathrm{AoA},\ell})\mathbf{a}_t^\dagger(\bar{\theta}^{(u)}_{\mathrm{AoD},\ell},\bar{\phi}^{(u)}_{\mathrm{AoD},\ell})\right], \quad (4)$$

where $\bar{\theta},\bar{\phi}$ denote the azimuth and elevation angles defined in a similar way as before but for the specular and scattered components, d_0 is the distance between the BS and UE, K is the Rice factor, N_p is the number of scattered paths, δ_u denotes the random phase of the specular component and $\beta_\ell^{(u)}$ is the complex Gaussian channel of the ℓ-th scattered path of the direct-link channel between the BS and UE u. Note that in the mmWave bands, $K>1$ and N_p should be small.

To model the angles, θ,ϕ, we utilize the sectoring concept in [14]. Hence, the probability density function of θ is

$$p_\Theta(\theta)=\begin{cases}\frac{1}{\Delta\theta} & \text{if } \theta^*-\frac{\Delta\theta}{2}\le\theta\le\theta^*+\frac{\Delta\theta}{2},\\ 0 & \text{otherwise,}\end{cases} \quad (5)$$

where $\theta^*\sim\mathcal{U}(0,2\pi)$ represents the mean angle, and $\Delta\theta$ is the parameter that dictates the directivity of the channel. For higher frequency, $\Delta\theta$ should be smaller. Similarly, ϕ can be modelled with its mean ϕ^* and range $\Delta\phi$. Note that if $d_1>d_2$, then the range of AoDs (i.e., ΔAoD) from the BS to a DASS is smaller than ΔAoA from the DASS to the UE.

Overall, the received signals at the FAS ports of UE u can be expressed in vector form as

$$\mathbf{r}_u=\underbrace{\left(\mathbf{G}_d^{(u)}+\sum_{n=1}^{N_{\mathrm{ris}}}\mathbf{H}_{n,u}\right)}_{\bar{\mathbf{H}}_u}\left(\sum_{\tilde{u}=1}^{U}\boldsymbol{\omega}_{\tilde{u}}s_{\tilde{u}}\right)+\boldsymbol{\eta}_u, \quad (6)$$

where $\bar{\mathbf{H}}_u$ represents the overall channel matrix from the BS to UE u, $\boldsymbol{\eta}_u$ denotes the complex additive white Gaussian noise (AWGN) vector with independent and identically distributed (i.i.d.) entires each following $\mathcal{CN}(0,\sigma_\eta^2)$, and $s_{\tilde{u}}$ denotes the symbol for UE $\tilde{u}$ transmitting using precoding vector $\boldsymbol{\omega}_{\tilde{u}}$. Note that the phases $\{\varphi_{n,m}\}$ at the DASSs are randomly generated while the optimization of $\boldsymbol{\omega}_{\tilde{u}}$ will be discussed later.

TABLE I
THE SIMULATION PARAMETERS SPECIFIC TO FREQUENCY.

f (GHz)	λ (cm)	W	Length (cm)‡	ΔAoD	ΔAoA
26	1.2	15	17	10°	30°
40	0.75	30	22	5°	10°

‡The length can be much shorter if a 2D FAS is considered.

TABLE II
OTHER SIMULATION PARAMETERS.

N	d_0 (m)	d_1 (m)	d_2 (m)	α_1	α_2	Γ (dB)
1000	100	70	40	4	2	10

For benchmarking, we define the average received signal-to-noise ratio (SNR) as $\Gamma=\frac{\sigma_s^2}{d_0^{\alpha_1}}$ if the direct link is present; otherwise, $\Gamma=\frac{\sigma_s^2}{d_1^{\alpha_1}d_2^{\alpha_2}}$, where $\sigma_s^2=\mathrm{E}[|s_u^2|]$ for all the UEs.

B. FAMA

At UE u, the best port k^* out of all the N ports is activated according to some criterion.[5] For slow FAMA, we have

$$k^*=\arg\max_k\frac{\sigma_s^2\left|\left[\bar{\mathbf{H}}_u\boldsymbol{\omega}_u\right]_k\right|^2}{\sigma_s^2\left|\left[\bar{\mathbf{H}}_u\sum_{\tilde{u}\neq u}\boldsymbol{\omega}_{\tilde{u}}\right]_k\right|^2+\sigma_\eta^2}, \quad (7)$$

which is analogous to [12, (4)]. In (7), the notation $[\mathbf{x}]_k$ obtains the k-th entry of $\mathbf{x}$. In the case of fast FAMA, we have

$$k^*=\arg\max_k\frac{\left|\left[\bar{\mathbf{H}}_u\boldsymbol{\omega}_u\right]_k\right|^2}{\left|\left[\bar{\mathbf{H}}_u\sum_{\tilde{u}\neq u}\boldsymbol{\omega}_{\tilde{u}}s_{\tilde{u}}+\boldsymbol{\eta}_u\right]_k\right|^2}, \quad (8)$$

which resembles [12, (5)]. How the instantaneous energy ratio in (8) can be estimated has been addressed in [15].

Given that a fixed rate is transmitted to every UE specified by an SINR threshold γ, the multiplexing gain is given by

$$m=U\left(1-\mathrm{E}_u\left[\mathrm{Prob}\left(\mathrm{SINR}_{u,k^*}<\gamma\right)\right]\right)\le U. \quad (9)$$

C. Precoding Design

In this letter, we consider the following precoding schemes.

- Identity precoding—Set $[\boldsymbol{\omega}_1\cdots\boldsymbol{\omega}_U]=\mathbf{I}$.
- Random precoding—Choose $[\boldsymbol{\omega}_1\cdots\boldsymbol{\omega}_U]$ randomly.
- SVD (singular-value decomposition) of $\mathbf{G}_d^{(u)}$—Select $\boldsymbol{\omega}_u$ as the right principal singular vector of the direct-link channel $\mathbf{G}_d^{(u)}$ for UE u.
- SVD of $\bar{\mathbf{H}}_u$—Select $\boldsymbol{\omega}_u$ as the right principal singular vector of the overall channel $\bar{\mathbf{H}}_u$ for UE u.

III. SIMULATION RESULTS

A. Setup

In this section, we provide and discuss the simulation results of the MIMO-FAMA downlink network with the aid of DASSs based on the system model described above. Two frequencies are considered and the simulation parameters are presented in TABLE I & II. All the BS antennas have the same mean AoD to a given DASS whose unit cells have the same mean AoA to a particular UE. The mean angles are randomly generated.

[5]More than one ports can be activated if more than one radio frequency (RF) chains are available. In that case, signal combining over multiple activated ports should be considered. We defer this study to future work.

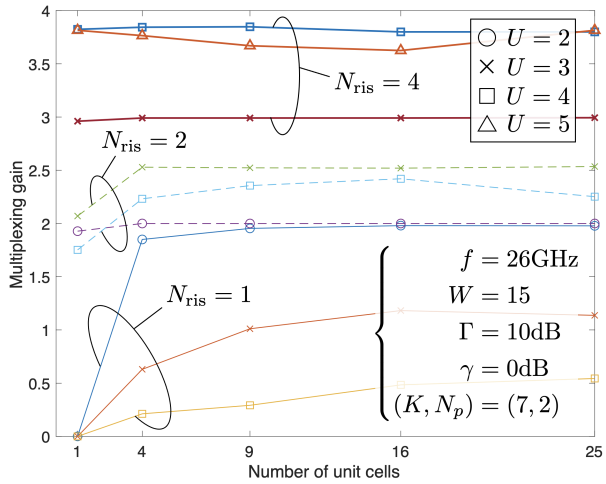

Fig. 2. Multiplexing gain of slow FAMA versus $N_{\rm cell}$ at $f=26$ GHz.

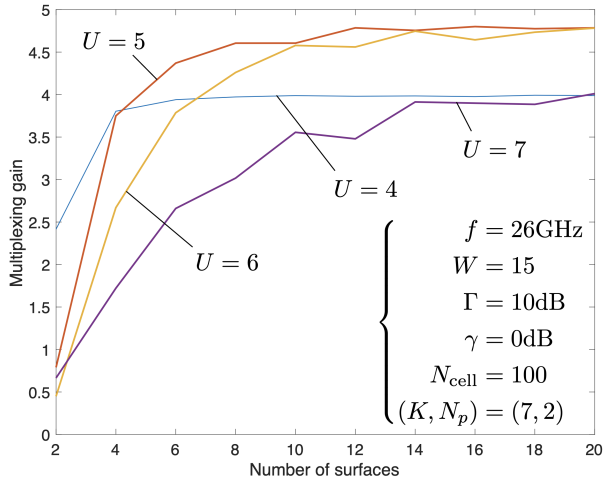

Fig. 3. Multiplexing gain of slow FAMA versus $N_{\rm ris}$ at $f=26$ GHz.

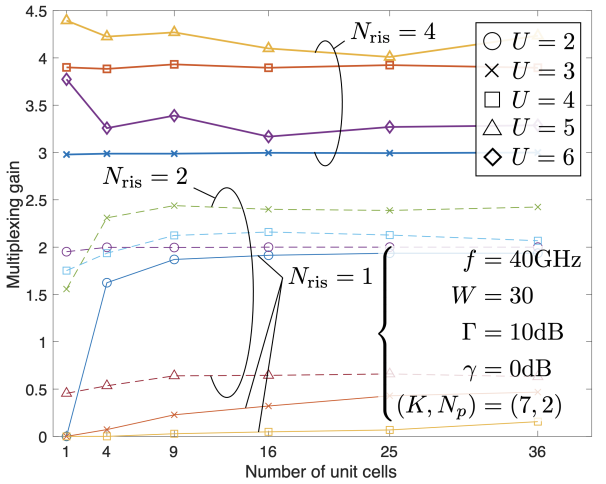

Fig. 4. Multiplexing gain of slow FAMA versus $N_{\rm cell}$ at $f=40$ GHz.

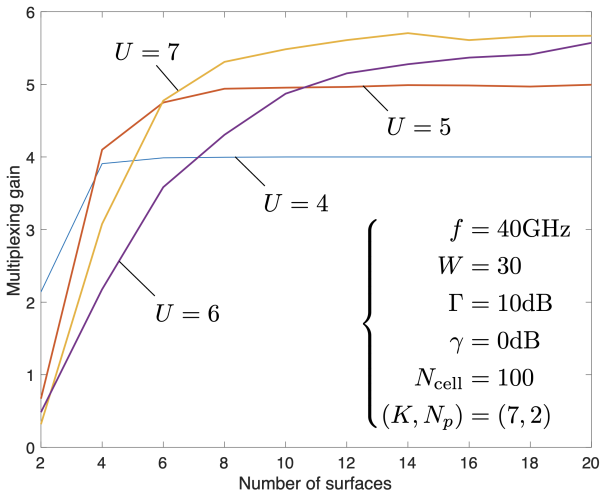

Fig. 5. Multiplexing gain of slow FAMA versus $N_{\rm ris}$ at $f=40$ GHz.

Note that a USA is adopted at the BS. Therefore, N_t is chosen as the minimum square number which is greater than or equal to U. Despite this, for identity or random precoding, only the first U BS antennas are used for transmission. Also, in all the figures except Fig. 6, identity precoding is employed. Figs. 2–6 study slow FAMA while Fig. 7 considers fast FAMA.

B. Multiplexing Gain against $N_{\rm cell}$ and $N_{\rm ris}$

Results in Figs. 2 and 3 are given for the multiplexing gain at 26 GHz against the number of unit cells, $N_{\rm cell}$, and the number of DASSs, $N_{\rm ris}$, respectively. The results indicate that the multiplexing gain increases with $N_{\rm cell}$ but saturates quite quickly. The reason is that the AoDs from the BS to the unit cells of a DASS and the AoAs from the unit cells to the UE have the same means. As such, the channels with an increased number of unit cells are highly correlated, which explains the diminishing return. By contrast, we see that the multiplexing gain can be much improved when $N_{\rm ris}$ increases. In addition, another observation is that the number of (co-channel) UEs cannot be excessively large because given the size, FAS may be unable to overcome the interference. Figs. 4 and 5 provide the corresponding results for 40 GHz where the results show even more promising multiplexing gain results. In summary, at 26 GHz, slow FAMA can achieve a multiplexing gain of 4.8 serving 5 co-channel UEs while at 40 GHz, slow FAMA can support 6 or 7 UEs to have a multiplexing gain of 5.7.

C. Precoding Comparison

Here, we investigate the importance of precoding design in the MIMO-FAMA system. Without providing the results, we like to point out that if the direct link does not exist, precoding optimization will fail. The reason is that all the UEs share the same channel from the BS to any DASS, any smart precoding trying to focus the signal power towards the DASS will not help in separating the UE signals. Secondly, normal precoding design usually expects the UE to have a beamforming vector matching to the transmit precoding in order to work. However, in FAMA, no beamforming is employed at the UE. Now, let us discuss the results in Fig. 6 when the direct link does exist. As we can see, precoding becomes important and increasing $N_{\rm ris}$ does only little in improving the performance further. By contrast, for random precoding, slow FAMA works well only if $N_{\rm ris}$ is large and even so U cannot be large. Another useful

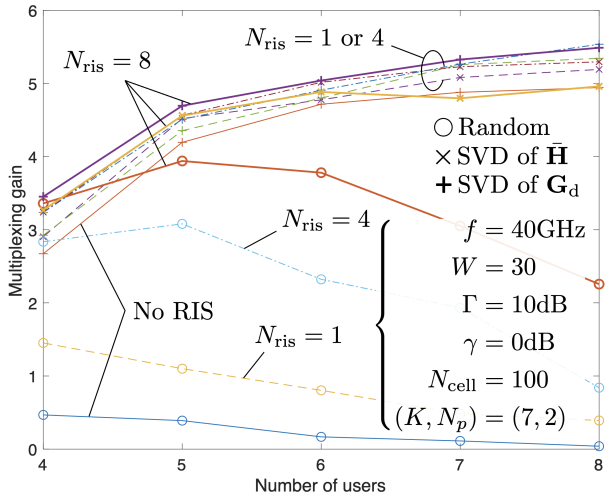

Fig. 6. Multiplexing gain of slow FAMA versus U for different precoding methods at $f = 40$ GHz when the direct link exists.

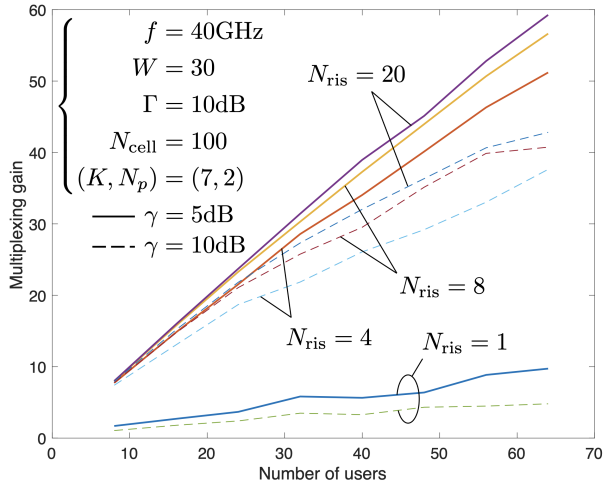

Fig. 7. Multiplexing gain of fast FAMA versus U at $f = 40$ GHz.

finding is that SVD precoding of the direct link channel works even better than that of the overall channel.

D. Massive Connectivity using Fast FAMA

So far, all the results discussed are for slow FAMA. In this subsection, we reveal what can be achieved if fast FAMA is considered by the results in Fig. 7 where the SINR threshold γ is raised to 5 or 10 dB. Identity precoding is assumed and no direct link exists. One remarkable finding here is that unlike slow FAMA, the multiplexing gain in fast FAMA increases linearly with the number of co-channel UEs, U. That is, more UEs do not mean higher difficulty to avoid interference. In fact, to the contrary, one could argue that more UEs contribute to creating interference null in (8). The results also indicate that evidently, a necessary condition for fast FAMA to function well is to have a good number of $N_{\rm ris}$, e.g., ≥ 4. Importantly, we should point out that if we continue to increase the number of users to $U = 100$, fast FAMA can deliver a multiplexing gain of 85.4 and 54.3 at $\gamma = 5$ and 10 dB, respectively.

We conclude this section by pointing out that recently, [16] draws a similar conclusion that RIS as a random reflector can be beneficial in creating the channel conditions for multiple access. In particular, it was shown that a random RIS reflector would increase channel orthogonality among the UEs allowing zero-forcing (ZF) to approach the performance of dirty-paper coding (DPC). However, the conclusion was limited to maintaining the use of ZF in place of the more complex DPC. By contrast, our results illustrate that even ZF is unnecessary if we have FAS at the UEs to handle the inter-user interference. In addition, it is worth mentioning that [16] bases its analysis using a rich-scattering channel model while the finite scatterer model in this letter is more suitable for mmWave channels.

IV. Conclusion

In this letter, we presented a new paradigm where RISs act as DASSs without optimization to realize massive connectivity of FAS-aided UEs. The results illustrated that a good number of DASSs effectively randomize the UE channels for FAMA. Without the direct link, BS precoding appears ineffective and FAMA is able to accommodate a large number of UEs.

References

[1] T. S. Rappaport *et al.*, "Wireless communications and applications above 100 GHz: Opportunities and challenges for 6G and beyond," *IEEE Access*, vol. 7, pp. 78729–78757, 2019.

[2] RCRWirelessNews, "Parsing the 5G power equation: Is 5G actually greener?," [Online] https://www.rcrwireless.com/20220124/5g/parsing-the-5g-power-equation-is-5g-actually-greener, Jan. 2022.

[3] N. Bhushan *et al.*, "Network densification: The dominant theme for wireless evolution into 5G," *IEEE Commun. Mag.*, vol. 52, no. 2, pp. 82–89, Feb. 2014.

[4] Y. Liu *et al.*, "Reconfigurable intelligent surfaces: Principles and opportunities," *IEEE Commun. Sur. & Tut.*, vol. 23, no. 3, pp. 1546–1577, 2021.

[5] M. A. ElMossallamy *et al.*, "Reconfigurable intelligent surfaces for wireless communications: Principles, challenges, and opportunities," *IEEE Trans. Cogn. Commun. Netw.*, vol. 6, no. 3, pp. 990–1002, Sept. 2020.

[6] S. Abadal, T. Cui, T. Low, and J. Georgiou, "Programmable metamaterials for software-defined electromagnetic control: Circuits, systems, and architectures," *IEEE J. Emerging and Select. Topics Circuits and Syst.*, vol. 10, no. 1, pp. 6–19, Mar. 2020.

[7] D. A. Urquiza Villalonga, H. OdetAlla, M. J. Fernández-Getino Garca, and A. Flizikowski, "Spectral efficiency of precoded 5G-NR in single and multi-user scenarios under imperfect channel knowledge: A comprehensive guide for implementation," *Electronics*, vol. 11, no. 24, p. 4237, Dec. 2022.

[8] Z. Wei, B. Li, and W. Guo, "Adversarial reconfigurable intelligent surface against physical layer key generation," [Online] arXiv:2206.10955, 2022.

[9] K. K. Wong, K. F. Tong, Y. Shen, Y. Chen, and Y. Zhang, "Bruce Lee-inspired fluid antenna system: Six research topics and the potentials for 6G," *Frontiers in Commun. and Netw., section Wireless Commun.*, 3:853416, Mar. 2022.

[10] K. K. Wong, D. Morales-Jimenez, K. F. Tong, and C. B. Chae, "Slow fluid antenna multiple access," to appear in *IEEE Trans. Commun.*, 2023.

[11] K. K. Wong, and K. F. Tong, "Fluid antenna multiple access," *IEEE Trans. Wireless Commun.*, vol. 21, no. 7, pp. 4801–4815, Jul. 2022.

[12] K. K. Wong, W. K. New, X. Hao, K. F. Tong, and C. B. Chae, "Fluid antenna system–Part I: Preliminaries," submitted to *IEEE Commun. Lett.*.

[13] R. W. Heath, N. González-Prelcic, S. Rangan, W. Roh and A. M. Sayeed, "An overview of signal processing techniques for millimeter wave MIMO systems," *IEEE J. Select. Topics Sig. Process.*, vol. 10, no. 3, pp. 436–453, Apr. 2016.

[14] A. Thornburg, T. Bai and R. W. Heath, "Performance analysis of outdoor mmWave ad hoc networks," *IEEE Trans. Sig. Process.*, vol. 64, no. 15, pp. 4065–4079, Aug. 2016.

[15] K. K. Wong, K. F. Tong, Y. Chen, and Y. Zhang, "Fast fluid antenna multiple access enabling massive connectivity," *IEEE Commun. Lett.*, vol. 27, no. 2, pp. 711–715, Feb. 2023.

[16] G. Chen, and Q. Wu, "Fundamental limits of intelligent reflecting surface aided multiuser broadcast channel," [Online] arXiv:2301.10526, 2023.